Dyslipidemia at the crossroad of the skin barrier and the arterial wall

Martins Cardoso, R.

Chapter 6

Complement receptor targeted liposomes encapsulating the liver X receptor agonist GW3965 accumulate in and stabilize atherosclerotic plaques

Advanced Healthcare Materials 9(10): 2000043 (2020).

Renata Martins Cardoso[1*], Naomi Benne[1*], Aimee L. Boyle[2], Alexander Kros[2], Wim Jiskoot[1], Johan Kuiper[1], Joke Bouwstra[1], Miranda Van Eck[1], Bram Slütter[1]

[1]Division of BioTherapeutics, Leiden Academic Centre for Drug Research, Leiden University, Leiden, The Netherlands
[2]Dept. Supramolecular & Biomaterials Chemistry, Leiden Institute of Chemistry, Leiden University, the Netherlands

*Both authors contributed equally

ABSTRACT

Atherosclerosis is the predominant underlying pathology of cardiovascular disease and is characterized by the retention of lipids, such as cholesterol, in macrophages (foam cells) in the intima of arteries. Liver X receptor agonists are promising compounds for treating atherosclerosis, since they induce reverse cholesterol transport in foam cells. However, LXR activation in the liver can lead to increased lipid levels. Therefore, in the present study we aimed to deliver LXR agonist GW3965 to atherosclerotic plaques by encapsulating it in liposomes. To increase the retention in atherosclerotic lesions, the liposomes were functionalized with the synthetic peptide Lyp-1 (CGNKRTRGC), which binds the p32 receptor on foam cells. Synthetic Lyp-1 was conjugated to DSPE-PEG2000-COOH and GW3965-containing (Lyp-1) liposomes (80 nm, PDI < 0.1, -20 mV) were prepared with nearly 100% encapsulation efficiency. Lyp-1 liposomes showed a 4-fold higher accumulation in foam cells compared to macrophages in vitro ($p < 0.05$). Moreover, in vivo targeting experiments showed significantly higher accumulation of Cy5-labeled Lyp-1 liposomes in atherosclerotic plaques compared to non-targeted liposomes, as shown by total (29-fold increase, $p < 0.01$) and relative radiant efficiency (25-fold increase, $p < 0.001$). Flow cytometric analysis demonstrated a 1.7-fold ($p < 0.05$) increase in the accumulation of Lyp-1 liposomes in atherosclerotic plaque macrophages as compared to controls. Finally, the effect of GW3965 loaded in Lyp-1 liposomes on atherosclerotic plaques was determined in low-density lipoprotein receptor knockout mice fed a western type diet for 13 weeks. Treatment with GW3965 loaded Lyp-1 liposomes twice a week for 5 weeks significantly reduced plaque macrophage content by nearly 50% ($p < 0.05$) and increased collagen content about 3-fold ($p < 0.01$) compared to PBS and free drug controls. Moreover, these changes in plaque stabilization were not accompanied by changes in plasma or hepatic lipid content. Thus, GW3965 loaded Lyp-1 liposomes successfully targeted the atherosclerotic plaque to allow plaque stabilization, in the absence of commonly observed side effects associated with the use of LXR agonists.

Keywords: *Lyp-1, foam cells, LXR, atherosclerosis, liposomes*

1. INTRODUCTION

Atherosclerosis is the predominant underlying pathology of cardiovascular disease and is one of the leading causes of death worldwide[1]. It is characterized by chronic inflammation in medium-and large-sized arteries caused by the subendothelial accumulation of oxidized low-density lipoprotein (oxLDL)[2]. This attracts immune cells, such as monocytes, which upon differentiation into macrophages clear oxLDL via scavenger receptors and can transform into large lipid-laden foam cells[3]. These foam cells are unable to migrate out of the vessel wall, leading to a build-up at the site of inflammation and the formation of atherosclerotic plaques[4].

There is increasing evidence that the migratory capacity of foam cells out of atherosclerotic plaques can be restored after cholesterol efflux[5]. Therefore, a promising treatment strategy to reverse the formation of foam cells is to stimulate this process[6]. Lipid-laden macrophages can actively transport excess cholesterol across their membrane via the ATP-binding cassette (ABC) transporters ABCA1 and ABCG1[7]. The liver X receptor (LXR) is a member of a family of nuclear transcription factors (LXRα; LXRβ) involved in the regulation of lipid homeostasis in response to altered sterol levels and controls the expression of both ABC transporters[7]. The deletion of these transcription factors in mice is associated with a remarkable increase in atherosclerotic lesions[8], implying therapeutic value of modulating LXR activity in atherosclerosis.

A class of small molecules, called LXR agonists (*e.g.* GW3965[9]), can activate this receptor to subsequently increase the efflux of excess cholesterol from foam cells via the induction of ABCA1 and ABCG1, reducing the local lipid content and enabling subsequent clearance of these cells from the plaque[10]. Several studies have demonstrated the beneficial effects of LXR agonists on reducing atherosclerotic plaque burden[11], however, LXR expression is not restricted to macrophages. LXRα is abundantly present in the liver, intestine, adipose tissue, spleen, and kidney[12] and LXRβ is ubiquitously expressed, although at a lower level. Therefore, when administered systemically, LXR agonists may affect several organs[12]. Activation of LXRα in the liver leads to high triglyceride levels in the plasma and liver[13-15]. This unwanted effect of LXR agonism could be prevented by altering the biodistribution of the active compound, directing it away from the liver and increasing the effective dose at the target site; the atherosclerotic lesion.

Encapsulation of active compounds in a drug delivery vehicle such as a nanoparticle is an effective strategy to alter their biodistribution[16]. In addition, conjugation of a targeting molecule to the drug delivery vehicle will direct the active compound to the required site of action[17]. Targeting to atherosclerotic plaques generally focuses on targeting to

endothelial cells1[8-22], clotted plasma proteins[23], or macrophages[24-26], by using HDL-like nanoparticles[27,28], or by passive targeting via sheer stress-mediated extravasation[29]. A common problem with many targeting strategies is lack of penetration into the plaque[22,23] or non-specificity[25,29].

The cyclic peptide Lyp-1 (CGNKRTRGC) has been identified as a valuable tool with a remarkable ability to penetrate into atherosclerotic plaques, making it superior for targeting macrophages in atherosclerotic plaques than other targeting peptides[30]. It binds to p32, also known as gC1q receptor, a receptor for the globular head domains of the complement component C1q. This receptor was originally found to be overexpressed on the cell surface of tumor cells[31] but is also expressed on foam cells in atherosclerotic plaques[32]. Nanoparticles coupled to Lyp-1 have been used for imaging of atherosclerotic plaques,[33,34] but so far, no studies have been performed using Lyp-1-targeted nanoparticles as treatment against atherosclerosis[35].

In this study, we aimed to design a particulate formulation combining the targeting properties of Lyp-1 with the therapeutic effect of an LXR agonist (GW3965) to promote cholesterol efflux from foam cells in atherosclerotic plaques to slow down atherosclerotic plaque development or reverse disease. We hypothesized that delivery of GW3965 with targeted liposomes will increase the retention of loaded particles in the atherosclerotic plaque, thereby reducing foam cell content in the plaque.

2. MATERIALS AND METHODS

2.1 Materials and chemicals

Rat and mouse no.3 breeding chow diet and Western-type diet (WTD) contained 0.25% cholesterol and 15% cocoa butter were purchased from Special Diet Services, Essex, UK. 1,2-dioleoyl-sn-glycero-3-phosphocholine (DOPC), DOPC-cyanine 5 (DOPC-Cy5), 1,2-dioleoyl-sn-glycero-3-phospho-L-serine (DOPS), 1,2-distearoyl-sn-glycero-3-phosphoethanolamine-polyethylene glycol (DSPE-PEG2000), and DSPE-N-[carboxy(polyethylene glycol)-2000] (DSPE-PEG2000-COOH) were purchased from Avanti Polar Lipids (Alabaster, AL, USA). O-(1H-6-chlorobenzotriazole-1-yl)-1,1,3,3-tetramethyluronium hexafluorophosphate (HCTU) and all amino acids used for synthesis were obtained from Novabiochem (Amsterdam, the Netherlands). N-N'-diisopropylethylamine (DIPEA) and Oxyma were purchased from Carl Roth (Karlsruhe, Germany). Dichloromethane (DCM) was obtained from Honeywell (Amsterdam, the Netherlands). Roswell Park Memorial Institute Medium (RPMI 1640), L-glutamine, and penicillin/streptomycin were purchased from Lonza (Basel, Switzerland). Fetal calf

serum (FCS) was bought from PAA Laboratories (Ontario, Canada) and polycarbonate track-etched pore size membranes (400 nm, 200 nm and 50 nm pore size) were obtained from Whatman® NucleoporeTM, GE Healthcare (Little Chalfont, UK). 70-µm cell strainer and 96-well plates were purchased from Greiner Bio-One B.V. (Alphen aan den Rijn, the Netherlands). Monosodium phosphate (NaH_2PO_4), disodium phosphate (Na_2HPO_4), diethyl ether, triisopropylsilane, iodine, diisopropylcarbodiimide, GW3965, Oil-red-O, Sirius Red, hematoxylin, NonidetTM P 40 Substitute, chloroform, collagenase I, collagenase XI, DNase, and hyaluronidase were purchased from Sigma-Aldrich (Zwijndrecht, The Netherlands). Dulbecco's Modified Eagle Medium (DMEM) low glucose, non-essential amino acids, pyruvate, oxidized LDL, Pierce™ BCA Protein Assay Kit, were purchased from ThermoFisher (MA, USA). Sodium chloride (NaCl) was obtained from Boom (Meppel, The Netherlands). Trifluoroacetic acid (TFA), piperidine, dimethylformamide (DMF), potassium dihydrogen phosphate (KH_2PO_4), potassium chloride (KCl), methanol and acetonitrile were purchased from Biosolve (Valkenswaard, the Netherlands). Optimal cutting temperature formulation Tissue-Tek®O.C.T. TM was purchased from Sakura Finetek (Alphen aan den Rijn, The Netherlands). Cholesterol and triglycerides colorimetric assays were obtained from Roche Diagnostics (Almere, The Netherlands). Rat anti-mouse macrophages/monocytes antibody (MOMA2) was purchased from Bio-Rad (Veenendaal, the Netherlands). Ketamine and atropine were purchased from AUV Veterinary Services (Cuijk, the Netherlands) and xylazine from ASTFarma (Oudewater, the Netherlands). CD45-AlexaFluor700 (30-F11) was obtained from Biolegend (San Diego, CA, USA). F4/80-FITC (BM8), fixable viability dye eFluor780, and MHC-II-eFluor450 (AF6-120.1) were purchased from eBioscience (San Diego, CA, USA). All solvents used were of analytical grade.

2.2 Animals

Wild-type (WT) and LDL receptor knockout ($LDLr^{-/-}$) mice on a C57BL/6 background were purchased from Jackson Laboratory (CA, USA), bred in-house under standard laboratory conditions, and provided with food and water ad libitum. Information about the diet used for individual experiments is described in each section. The regular laboratory diet (chow) was rat and mouse no.3 breeding diet. WTD contained 0.25 wt% cholesterol and 15 wt% cocoa butter. Animals had access to water and food ad libitum. All animal work was performed in compliance with the Dutch government guidelines and the Directive 2010/63/EU of the European Parliament. Experiments were approved by the Ethics Committee for Animal Experiments of Leiden University.

2.3 DSPE-PEG2000-Lyp-1 synthesis

The Lyp-1 peptide, GCGNKRTRGC with Cys residues protected by the non-acid-labile acetamidomethyl group, was synthesized using a Liberty Blue microwave-assisted peptide synthesizer. The synthesis was performed on a 0.1 mmol scale with a low-loading (0.18 mmol/g) tentagel R-RAM resin. Amino acid activation was achieved by using N,N'-diisopropylcarbodiimide as the activator and Oxyma as the base, while Fmoc-deprotection was achieved with 20% piperidine in DMF. Once the synthesis was complete, the resin was treated with 10 equivalents of iodine for one hour, to accommodate the concomitant deprotection and cyclization of the Cys residues. The resin was subsequently washed five times with DMF, five times with 2% acetic acid in DMF, five times with DMF and finally five times with DCM. The DSPE-PEG2000-COOH was manually coupled, on resin, to the N-terminus of an excess of the cyclized Lyp-1 by HCTU and DIPEA. The coupling reaction was left overnight, and the resin was subsequently washed with DMF and DCM. The DSPE-PEG2000-Lyp1 was cleaved from the resin by using a mixture of 97% TFA and 3% triisopropylsilane. The cleavage reaction was left to proceed for one hour, and the peptide was precipitated into ice-cold diethyl ether. The precipitate was collected by centrifugation. Levels of precipitate were low, likely due to the hydrophobic nature of the lipopeptide, therefore after centrifugation, the ether was separated from the precipitate and the ether was evaporated, leaving a white residue. This residue was combined with the original precipitate, dissolved in a mixture of acetonitrile and water, and dialyzed in a solution of 90% water and 10% acetonitrile to remove the excess uncoupled peptide and any scavengers or impurities that remained. The product was subsequently freeze-dried and analyzed using MALDI mass spectrometry to confirm the desired product had been formed.

2.4 Liposome preparation

Liposomes were prepared by using the thin film dehydration-rehydration method, as described previously[36]. Briefly, DOPC:DOPS:DSPE-PEG:DSPE-PEG-Lyp-1 in the molar ratio 76:19:4.3:0.7 were dissolved in chloroform and mixed in a round-bottom flask to obtain a final lipid concentration of 10 mg/mL. To this mixture, 2 mg of GW3965 was added. Chloroform was evaporated for 1 hour at 40°C in a rotary evaporator (Rotavapor R-210, Büchi, Switzerland). The lipid film was rehydrated with 1 mL Milli-Q water and homogenized by using glass beads and gentle swirling at room temperature (RT). The liposome dispersion was subsequently snap-frozen in liquid nitrogen, followed by freeze-drying overnight (Christ alpha 1–2 freeze-dryer, Osterode, Germany). The resulting dry lipid cake was gradually rehydrated at RT by using 10 mM phosphate buffer, pH 7.4 (PB); two volumes of 500 µL and one volume of 1000 µL PB were

successively added, with intervals of 30 min between each addition. The mixture was vortexed well between each hydration step, and the resulting dispersion was kept at RT for at least 1 hour. To obtain monodisperse liposomes, the multilamellar vesicles were sized by high-pressure extrusion at RT (LIPEX Extruder, Northern Lipids Inc., Canada). The liposome mixture was passed four times through stacked 400 nm and 200 nm polycarbonate track-etched pore size membranes and a further eight times through a 50 nm pore size membrane. To prepare fluorescently labeled liposomes, 0.1 mol% of DOPC was replaced with DOPC-Cy5. Liposomes were stored at 4°C and used for further experiments within 1 week.

2.5 Liposome characterization

The Z-average diameter and polydispersity index (PDI) of the liposomes were measured by dynamic light scattering (DLS) using a NanoZS Zetasizer (Malvern Ltd., Malvern, UK). Zeta-potential of the liposomes was determined by laser Doppler electrophoresis with the same instrument. Liposomes were diluted 100-fold in PB to a total volume of 1 mL prior to measuring. To determine the concentration of encapsulated GW3965 and Lyp-1, samples were analyzed by reversed-phase UPLC (Waters ACQUITY UPLC, Waters, MA, USA). 20 µL of the liposome dispersion was dissolved in 180 µL methanol. 10 µL of the sample was injected into a 1.7 µm BEH C18 column (2.1 x 50 mm, Waters ACQUITY UPLC, Waters, MA, USA). The column temperature and the temperature of the sample were set at 40°C and 4°C, respectively. The mobile phases were Milli-Q water with 0.1% TFA (solvent A) and acetonitrile with 0.1% TFA (solvent B). For detection, the mobile phases were applied in a linear gradient from 5% to 95% solvent B over 10.5 minutes at a flow rate of 0.370 mL/min. Lyp-1 was detected by absorbance at 220 nm using an ACQUITY UPLC TUV detector (Waters ACQUITY UPLC, Waters, MA, USA) and GW3965 was detected at 272 nm.

2.6 Bone marrow-derived macrophage (BMM) and foam cell culture

Bone marrow was isolated from the tibias and femurs of WT or $LDLr^{-/-}$ mice on a chow diet. The isolated bone marrow was passed through a 70-µm cell strainer. To differentiate the bone-marrow derived cells into macrophages, the cells were cultured in mixture of 60% complete RPMI medium (20% (v/v) FCS, 2 mM L-glutamine, 1 mM non-essential amino acids, 1 mM pyruvate, and 100 U/mL penicillin/streptavidin with 40% complete L929-conditioned DMEM low glucose medium (10% (v/v) FCS, 2 mM L-glutamine, and 100 U/mL penicillin/streptavidin) at 37˚C and 5% CO_2 for 7 days, as described previously[37]. The medium was refreshed every other day. To generate foam cells, macrophages were incubated with 75 µg/mL oxLDL for 30 hours.

2.7 Liposome association to BMMs and foam cells

BMMs and foam cells were cultured as described above. After 10 days of culture, 100,000 BMMs or foam cells were plated in 96-well plates and fluorescently labeled Lyp-1 liposomes or controls (PBS and fluorescently labeled non-targeted liposomes) were added at a concentration of 0.35 mg/mL Lyp-1 or an equivalent lipid dose. After 2 hours of incubation at 37˚C and 5% CO_2, excess liposomes were removed by washing the cells several times with medium. Cells were stained for F4/80 and viability dyes and were analyzed by flow cytometry (CytoFLEX S, Beckman Coulter, CA, USA). Data were analyzed by using FlowJo software (Treestar, OR, USA).

2.8 *In vivo* targeting to atherosclerotic plaques

Male $LDLr^{-/-}$ mice (6 to 10-week old) were fed WTD for 13 weeks to stimulate atherosclerotic lesion development. Subsequently, the mice were randomized into two groups (n = 10) injected intravenously with either Cy-5 fluorescently labeled non-targeting liposomes or Lyp-1 targeting liposomes (200 µL).The Lyp-1 concentration was 35 µg for Lyp-1 liposomes, and the equivalent lipid concentration was used for non-targeted liposomes. After 3 hours, the mice were anesthetized by using a mixture of ketamine (40 mg/mL), atropine (50 µg/mL), and sedazine (6.25 mg/mL) and perfused with PBS (8.13 g/L NaCl, 2.87 g/L Na_2HPO_4, 0.2 g/L KH_2PO_4, 0.19 g/L KCl, pH 7.4) via the left ventricle of the heart under physiological pressure after opening the thoracic cavity. After perfusion, the mice were imaged by using a fluorescence in vivo imaging system (IVIS, Perkin-Elmer IVIS Lumina Series III, Waltham, MA, USA) to provide information about the biodistribution of the liposomes. Afterward, spleen, lungs, liver, kidneys, hearts, and aortas were also imaged separately. Uptake by different organs was plotted as radiant efficiency and as relative radiant efficiency (%). To calculate relative radiant efficiency, the total sum of signals in organs was set to 100%, and the relative percentage per organ was calculated from this value. Aortas were further processed for flow cytometry analysis, as previously described[38]. Briefly, aortas were cut into small pieces, incubated with 450 U/mL collagenase I, 250 U/mL collagenase XI, 120 U/mL DNase, and 120 U/mL hyaluronidase (30 min at 37°C under constant agitation), and strained through a 70-µm cell strainer to obtain a single-cell suspension. Cells were stained for CD45, F4/80, MHC-II, and viability and analyzed by flow cytometry.

2.9 Analysis of atherosclerosis in mice

Male $LDLr^{-/-}$ mice (6 to 10-week old) were fed WTD for 8 weeks to develop atherosclerotic lesions. Next, these mice were randomized into 5 groups (n = 10 mice)

to receive intravenous injections twice a week (200 µL) of (1) PBS; (2) free GW3965; (3) empty Lyp-1 liposomes; (4) GW3965-loaded liposomes or (5) GW3965-loaded Lyp-1 liposomes. For GW3965-containing groups the dose was 6.5 mg/kg GW3965. The mice were treated for 5 weeks and continued to receive WTD during this time. After 5 weeks of treatment, the mice were anesthetized, exsanguinated and perfused, as described in the previous section. Hearts, livers, and blood were collected for further analysis. Hearts were embedded in OCT and stored at -80°C until further processing. Cryosections of the aortic root (10 µm, CM3050S cryostat, Leica, Rijswijk, The Netherlands) were collected. The sections were stained for Oil-Red-O to visualize lipid-rich plaques[39]. The largest Oil-red-O positive section of a sample and the two flanking sections were used to quantify the average plaque size. Macrophage positive area in the plaque was determined by using MOMA2 staining[40]. Macrophage positive area was calculated as the area positive for the MOMA2 staining divided by the total plaque area for the 3 largest consecutive sections. Collagen content in the plaques was measured by using Sirius Red staining[41]. Sections were visualized under polarized light[42] and the collagen content was determined by dividing the area positive for the Sirius Red staining by the total plaque area for the 3 largest consecutive sections. All stainings were imaged by using a Leica DM-RE microscope (Leica, Imaging Systems, UK) and analyzed using Leica QWin software.

2.10 Lipid quantification

Triglycerides were extracted from liver samples (± 50 mg tissue) homogenized with NonidetTM P 40 Substitute. To solubilize the triglycerides in the homogenate, the samples underwent two cycles of heat (90°C) and chill on ice. Subsequently, the homogenates were centrifuged (14000 rpm) to remove insoluble material and triglycerides were measured by a colorimetric enzymatic assay[43]. The Folch method[44] was used to extract cholesterol from liver samples (ca. 50 mg tissue). Cholesterol was then quantified by using a colorimetric enzymatic assay[43]. Both triglyceride and cholesterol levels were corrected for total protein concentration. Protein concentration was determined with a Pierce™ BCA Protein Assay Kit according to the manufacturer's instructions. Non-fasted plasma levels of cholesterol and triglycerides were measured by enzymatic colorimetric assays, as previously described by Out *et. al.*[43].

2.11 Statistical analysis

Statistical analysis was performed by using GraphPad Prism 8 (GraphPad Software Inc., CA, USA). Data are presented as mean ± standard deviation (SD) and *p* values below 0.05 were considered significant. For comparison of multiple treatment groups, unpaired

t-test, one-way ANOVA with Holm-Sidak post-test, or two-way ANOVA with Bonferroni's post-test were used, where appropriate.

3. RESULTS

3.1 Characterization of Lyp-1 starting materials and liposomes

The coupling reaction of cyclic Lyp-1 to DSPE-PEG2000-COOH generating DSPE-PEG2000-Lyp-1 is schematically represented in Figure 1 and was confirmed by MALDI-MS (Supplementary Figure S1). All GW3965-loaded liposomes showed an encapsulation efficiency of this drug of nearly 100% (Table I). The Z-average diameter of GW3965-loaded liposomes (ca. 75 nm) was slightly, but significantly ($p < 0.05$) smaller than that of empty liposomes (ca. 85 nm) (Table 1). The PDI was ca. 0.1 for all formulations, and the ζ-potential was about -20 mV (Table 1).

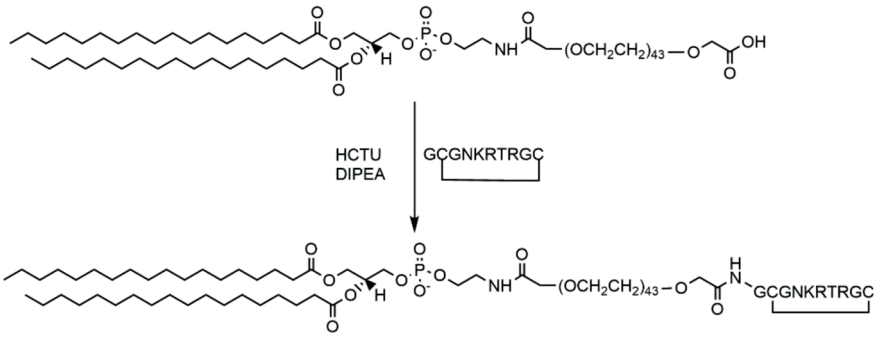

Figure 1. Synthesis of DSPE-PEG2000-Lyp-1. Schematic representation of the reaction coupling DSPE-PEG2000-COOH to cyclic peptide Lyp-1 to produce DSPE-PEG2000-Lyp-1.

Table 1: Physicochemical properties of liposomal formulations. Average particle diameter (Z-average diameter), PDI and ζ-potential were determined for all liposomal formulations. Encapsulation efficiency was calculated for liposomes loaded with GW3965 compound.

Formulation	Z-average diameter ± SD (nm)	PDI ± SD	ζ-potential ± SD (mV)	Encapsulation efficiency ± SD (%)
Empty Lyp-1 Liposomes	84.7 ± 3.9	0.09 ± 0.02	-19.3 ± 2.3	-
GW3965-loaded liposomes	73.8 ± 4.9*	0.10 ± 0.02	-19.7 ± 2.3	93.5 ± 19.9
GW3965-loaded Lyp-1 liposomes	77.5 ± 4.0*	0.09 ± 0.02	-19.5 ± 2.1	92.9 ± 22.5

*$p < 0.05$ compared to empty Lyp-1 liposomes

3.2 Lyp-1 liposomes preferentially associate with foam cells *in vitro*

To test the specific association of the liposomes to foam cells *in vitro*, fluorescently labeled liposomes were incubated with LDLr$^{-/-}$ mouse-derived non-differentiated BMMs (M0) and oxLDL-laden foam cells for 2 hours. Flow cytometric analysis showed that both non-targeted and targeted liposomes did not associate with M0 macrophages (Figure 2). Consistent with previous reports[22], foam cells showed enhanced association with both targeted and non-targeted liposomes. However, the interaction of Lyp-1 targeted liposomes was significantly increased as compared to not-targeted liposomes, marked by a higher fluorescent signal (Figure 2A and Figure 2B) and a nearly 4-fold increase in the percentage of liposome positive foam cells ($p < 0.05$) (Figure 2C). Similar results (4-fold increase, $p < 0.01$) were observed for M0 macrophages and foam cells both derived from WT mice containing a functional LDLr (data not shown).

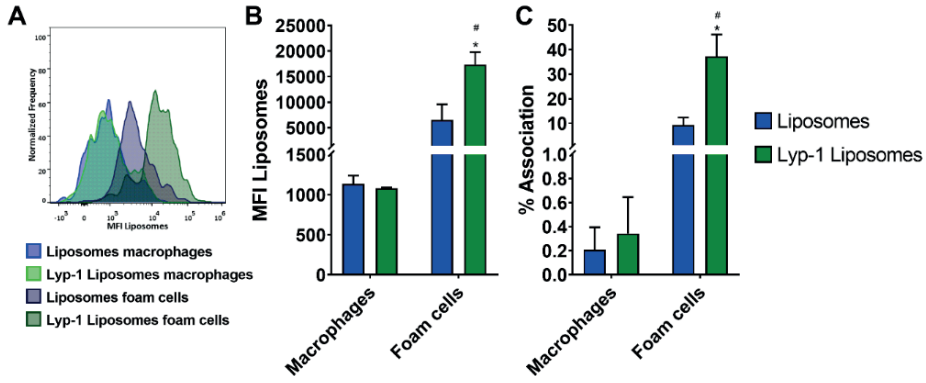

Figure 2. Preferential association of targeted Lyp-1 liposomes to foam cells in vitro. LDLr$^{-/-}$ M0 macrophages and oxLDL-laden foam cells were exposed to non-targeted liposomes or Lyp-1 liposomes labeled with DOPC-Cy5. After 2 hours of incubation, the liposomal association was determined by using flow cytometry. A) Representative MFI plots. Cell association was expressed as B) mean fluorescence intensity of the cells and C) percentage of cells positive for the fluorescent label. Graphs show means + SD of 3 independent experiments, *$p < 0.05$ comparing foam cells to M0 macrophages, #$p < 0.05$ comparing non-targeted to targeted liposomes, determined by two-way ANOVA and Bonferroni's post-test.

3.3 Lyp-1 liposomes are retained in plaque-residing foam cells of LDLr$^{-/-}$ mice

Next, we addressed the ability of the Lyp-1 liposomes to accumulate in foam cells residing in atherosclerotic plaques in vivo. LDLr$^{-/-}$ mice fed a WTD for 13 weeks were injected intravenously with fluorescently labeled Lyp-1 liposomes or non-targeted

liposomes. After 3 hours, mice were anesthetized and perfused, and the biodistribution of liposomes was assessed using fluorescence imaging (see Figure 3A and 3B for representative aortas) and flow cytometry (see Figure 3C and 3D for representative plots). Lyp-1 liposomes showed a significantly higher accumulation in atherosclerotic plaques compared to non-targeted liposomes, as shown by the total radiant efficiency (29-fold increase, $p < 0.01$, Figure 3E) and the relative fluorescence signal (25-fold increase, $p < 0.001$, Figure 3F). Flow cytometric analysis confirmed a 1.7-fold ($p < 0.05$) increase in the accumulation of Lyp-1 targeted liposomes in atherosclerotic plaque foam cells as compared to non-targeted control liposomes (Figure 3G). In addition, to determine the organ distribution of the liposomes, the liver, kidneys, heart, spleen, and lungs were collected and separately imaged with IVIS. Most liposomes (both targeted and non-targeted) accumulated in the spleen, liver and kidneys, and a small amount was recovered from the lungs and hearts (Figure S2). LDLr$^{-/-}$ mice that received chow diet instead of WTD, and therefore did not develop atherosclerotic plaques, did not show any liposomal signal in aortas (data not shown).

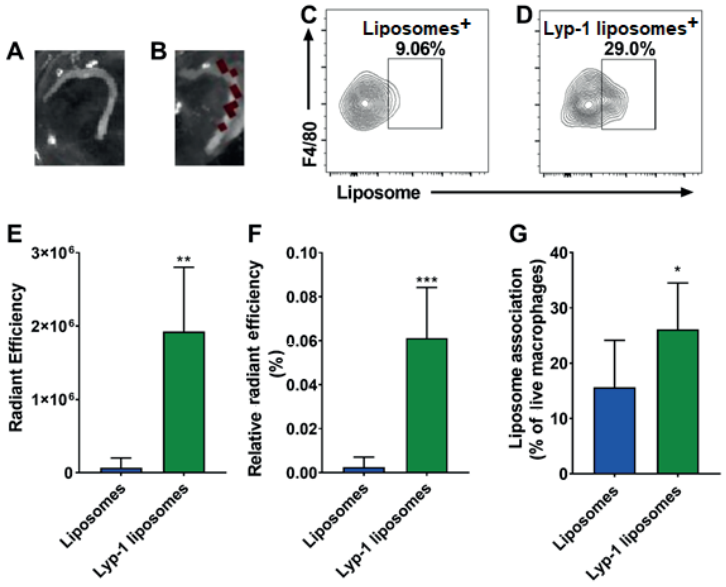

Figure 3. Association of fluorescently labeled non-targeted liposomes and Lyp-1 liposomes by plaque-residing foam cells in LDLr$^{-/-}$ mice fed WTD for 13 weeks. 3 hours after intravenous injection of liposomes, mice were perfused with PBS (pH 7.4 at RT). Representative IVIS images of descending aortas of mice that had received A) non-targeted and B) Lyp-1 liposomes. The dark brown signal indicates the presence of the Cy5 label. Representative FACS plots of pre-gated CD45^{+}MHC-II^{+}F4/80^{+} cells isolated from the aortic arch associated with C) non-targeted and D) Lyp-1 liposomes. E) Radiant efficiency of the fluorescent label in the descending aortas of mice measured by fluorescence imaging, n = 5. F) Aortic radiant efficiency as a

percentage of all organs, n = 5. G) Liposomes detected in $CD45^+MHC\text{-}II^+F4/80^+$ cells isolated from the aortic arch by flow cytometry, n = 8. Graphs show mean + SD, *p < 0.05, **p < 0.01, ***p < 0.001 determined by unpaired Student's T-test.

3.4 Treatment with GW3965-loaded Lyp-1 liposomes significantly reduces the macrophage content and increases the collagen content of atherosclerotic plaques

After confirming efficient targeting of the Lyp-1 liposomes to atherosclerotic foam cells, the effect of Lyp-1 liposomal targeting of the LXR agonist GW3965 on pre-established atherosclerotic lesions was assessed. Male $LDLr^{-/-}$ mice were fed WTD for eight weeks. At this point, the average plaque size in the aortic root area was ca. 0.12 ± 0.07 mm^2, with lesion area comprising of 57.1 ± 15.2% macrophages, and 1.3 ± 1.1% collagen. Subsequently, the mice were injected intravenously twice a week with PBS, free GW3965, empty Lyp-1 liposomes, GW3965-loaded liposomes or GW3965-loaded Lyp-1 liposomes for 5 weeks, during which the WTD was maintained. Upon sacrifice, no differences were observed in atherosclerotic plaque size between any of the groups as determined in Oil-red-O stained sections of the aortic roots (Figure 4A and 4D). However, the macrophage content, as measured with MOMA2 staining, was 2-fold ($p < 0.05$) lower in mice treated with Lyp-1 targeted GW3965-loaded liposomes compared to all other groups (Figure 4B and 4E). Previous studies have shown a positive correlation between the reduction in macrophage content and increase in collagen content in the plaque[45]. Indeed, we found that the percentage of collagen in the plaques was significantly increased (3-fold, $p < 0.01$) in mice treated with GW3965-loaded Lyp-1 liposomes as compared to all other groups (Figure 4C and 4F). Thus, foam cell delivery of GW3965 using Lyp-1 liposomes induced stabilization of established atherosclerotic plaques.

3.5 Free or encapsulated GW3965 does not affect plasma and liver lipid content

Despite the positive effects of LXR activation on atherosclerosis, the use of LXR agonists, such as GW3965, has been described to alter hepatic lipid metabolism often leading to an increase in circulating triglycerides and liver steatosis[10]. Triglyceride and cholesterol content (in both plasma and liver) showed no differences between any of the groups (Figure 5), suggesting that the GW3965 treatment with Lyp-1 targeted liposomes can stabilize atherosclerotic plaques without the confounding effects on serum and liver lipid levels.

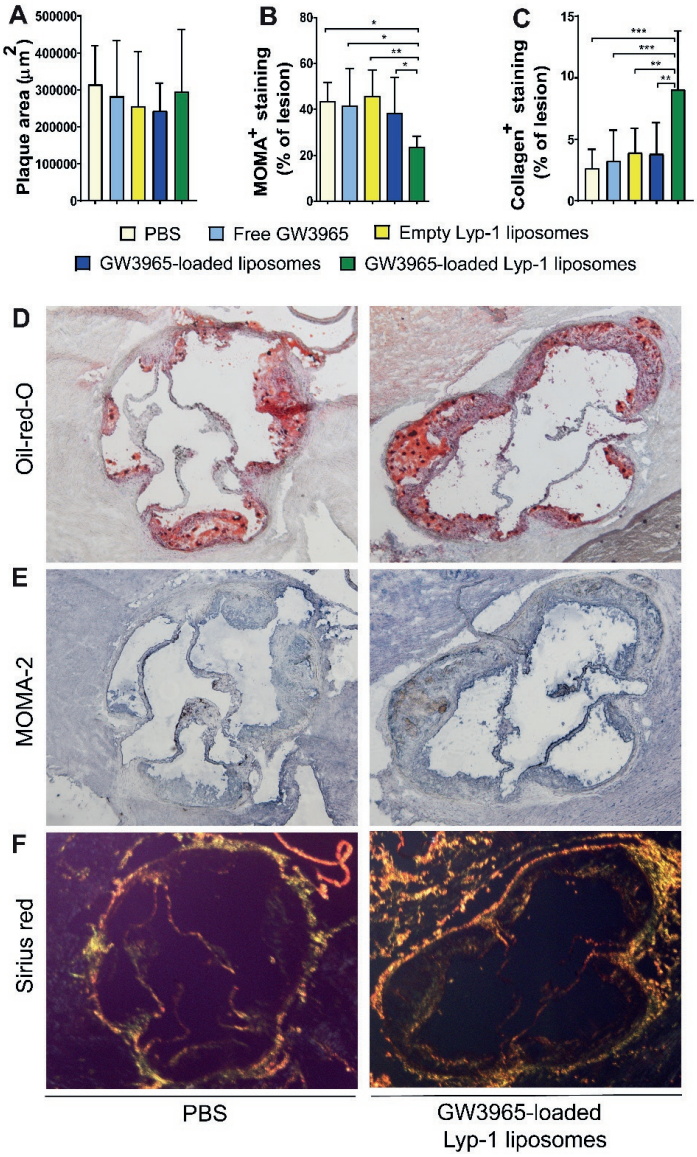

Figure 4. Effect of GW3965-loaded Lyp-1 targeted liposomes on plaque development in LDLr$^{-/-}$ mice. Mice were fed WTD for eight weeks before receiving intravenous injections of GW2965-loaded Lyp-1 liposomes or controls twice a week for five weeks while maintaining WTD. Upon sacrifice, hearts were collected and sectioned to reveal the aortic root area. Sections were stained for (A) Oil-Red-O to visualize lipids (B) MOMA2 to measure macrophage content, and (C) Sirius Red for collagen content, n = 10. Representative images of section stained for (D) Oil-red-O, (E) MOMA2 and (F) Sirius Red. Graphs show means + SD, *$p < 0.05$, **$p < 0.01$, ***$p < 0.001$ determined by one-way ANOVA with Holm-Sidak post-test.

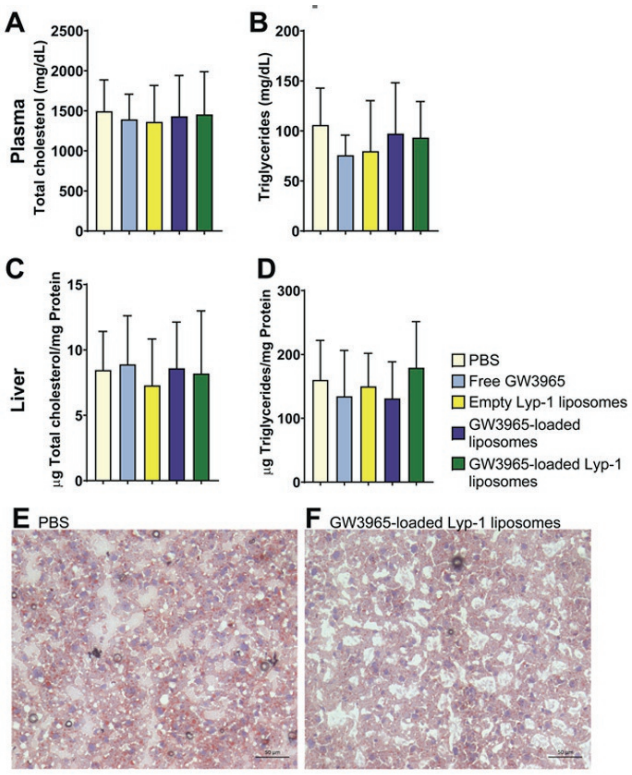

Figure 5. Effect of drug-loaded targeted liposomes and controls on plasma- and liver lipid levels in LDLr$^{-/-}$ mice on WTD. Mice received WTD for eight weeks before receiving intravenous injections of liposomes or controls twice a week for five weeks while maintaining WTD. Mice received the last injection 3 hours prior to sacrifice. Upon sacrifice, plasma and livers were collected for lipid analysis. (A) Total cholesterol and (B) triglyceride levels were measured in plasma. Livers were processed and total protein content in mg was determined. (C) Total cholesterol and (D) triglyceride levels were measured and normalized to protein content. (E) Representative image of Oil-Red-O stained liver of a mouse that received PBS, or (F) drug-loaded targeted liposomes, n = 10. Graphs show mean + SD, no significant differences found between groups.

4. DISCUSSION

LXR agonists are promising compounds for the treatment of atherosclerosis, but at therapeutic doses, they increase plasma triglyceride and cholesterol levels[13-15]. In this study, we showed that loading of an LXR agonist, GW3965, in Lyp-1-bearing liposomes induces a highly relevant stabilization of pre-established atherosclerotic lesions, in contrast to free GW3965 or GW3965 encapsulated in non-targeted liposomes. This is hypothesized to be due to the migration of macrophages out of lesions after LXR-agonist-

induced cholesterol efflux[5]. Liposomes consisting of DOPC:DOPS:DSPE-PEG:DSPE-PEG-Lyp-1 in a molar ratio of 76:19:4.3:0.7 were prepared to produce particles with fluid state membranes to improve the encapsulation of GW3965 and to prevent mononuclear phagocyte uptake upon injection into the circulation. Phosphatidylserine was added because of its anti-inflammatory properties[46-50] and reported ability to target foam cells[25]. Liposomes were PEGylated (5 mol%) to enhance their circulation time[51].

To minimize the undesired hepatic and metabolic effects, LXR agonists can be encapsulated into functionalized nanoparticles to target atherosclerotic plaques. Zhang *et. al.* formulated GW3965 in PEGylated PLGA nanoparticles containing phosphatidylserine on the surface to target atherosclerotic foam cells. The targeted PLGA particles (10 mg/kg GW3965; administered i.v. 3 times per week for 2 weeks) reduced the macrophage content in the lesion compared to untreated control. However, this effect was not enhanced when compared to free drug or drug encapsulated in non-targeted liposomes and was accompanied by increased hepatic and plasma triglyceride and cholesterol levels[25]. In a different approach, Yu *et. al.* encapsulated GW3965 in methoxy-PLA nanoparticles coated with 1,2-dilauroyl-sn-glycero-3-phosphocholine (DLPC):DSPE-PEG1000 functionalized with collagen-IV-targeting heptapeptide conjugated to DSPE-PEG2000 in the lipid layer. The GW3965-loaded collagen-targeting particles (8 mg/kg, administered intravenously 2 times per week for 5 weeks) significantly decreased the $CD68^+$ (macrophage) area in the lesion compared to free drug and non-targeted liposomes[18]. Neither of these previously described targeting approaches using collagen-IV and phosphatidylserine resulted in a reduction in total plaque size. Furthermore, the collagen content in the plaques, an important indicator of plaque stability, was not measured in these studies. It should be noted that, while in humans foam cells are mainly derived from macrophages[52], it has recently been discovered that foam cells can be derived from smooth muscle cells in the $ApoE^{-/-}$ mouse model[53]. Since the aforementioned studies and the study presented here are performed in $LDLr^{-/-}$ mice, it is unknown whether the therapeutic effect would be the same in $ApoE^{-/-}$ mice.

In this study, we made use of the interaction between the p32 receptor and Lyp-1 to target liposomes to foam cells in the plaque and deliver GW3965. Since the p32 receptor is not expressed on the surface of lipid-poor macrophages[31], the presence of Lyp-1 on the liposomal surface did not affect the in vitro association of the liposomes to undifferentiated macrophages but greatly and significantly enhanced their association to foam cells, confirming the selectivity of the targeting peptide. It should be noted that p32 has been found to be expressed in endothelial cells, foam cells, smooth muscle cells, and inflammatory cells present in the intima and media of human atherosclerotic

lesions[32]. However, similarly to the Lyp-1 liposomes described here, heat shock protein cages functionalized with Lyp-1 designed by Uchida *et. al.* showed accumulation in Mac-3^{+} foam cells in murine ligation-induced atherosclerotic plaques[33]. Seo *et. al.* also observed high aortic lesion retention of Lyp-1 dendrimers 3 hours after intravenous injection in ApoE$^{-/-}$ mice[34]. Remarkably, in our study, the presence of Lyp-1 on the liposomal surface leads to enough particle retention in the aorta to allow a clear therapeutic effect of a relatively low dose of GW3965 (ca. 6.5 mg/kg/injection). For reference, oral administration of high dose of free GW3965 (10 mg/kg) for 12 weeks significantly reduced lesion size. However, this effect was accompanied by higher serum triglycerides levels[14].

Administration of free or nanoparticle-encapsulated LXR agonist may not fully prevent unwanted effects in the plasma and in the liver[10]. In the present study, the high hepatic uptake of our GW3965-loaded Lyp-1 liposomes did not lead to the side effects typically associated with LXR agonists. Joseph *et. al.* showed that treatment with free GW3965 at a low dose (1 mg/kg for 12 weeks) did not result in plaque size reduction, hypertriglyceridemia or liver steatosis. The administration of a moderate dose of GW3965 (6.5 mg/kg in this study, *vs* 10 mg/kg by Zhang *et. al.*[25] and 8 mg/kg by Yu e*t. al.*[18]) may have contributed to maintenance of hepatic and serum lipid homeostasis, as free GW3965 also did not induce these unwanted effects. The aforementioned studies along with our own study demonstrate that uptake of nanoparticles by cells in the liver is difficult to avoid, especially by Kupffer cells[54], but nanoparticles can still protect against the unwanted effects of the LXR agonist while increasing the efficiency of the drug at the site of action. Nevertheless, high hepatic particle uptake in the long-term, especially with higher doses should be avoided. Thus, other liposomal formulations or even other types of particles could be explored to reduce the undesired particle removal by the liver.

In conclusion, our work shows that functionalizing liposomes with Lyp-1 is an excellent strategy for targeting to atherosclerotic plaques. We are, to our knowledge, the first to combine this targeting approach with an LXR agonist, and we show that GW3965 loaded in targeted liposomes can reduce plaque macrophage content and increase plaque stability. These findings suggest that it is possible to increase the efficacy of this LXR agonist and may contribute to the development of better atherosclerosis therapies.

ACKNOWLEDGMENTS

The authors thank P. J. van Santbrink, J. van Duijn, A. C. Foks, F. Lozano Vigario, R. J. T. Leboux, J. de Mol and I. Bot for their technical assistance during the animal studies.

REFERENCES

1. Frostegård, J. Immunity, atherosclerosis and cardiovascular disease. BMC Med 11, 117-117, doi:10.1186/1741-7015-11-117 (2013).

2 Pirillo, A., Norata, G. D. & Catapano, A. L. LOX-1, OxLDL, and atherosclerosis. Mediators Inflamm 2013, 152786, doi:10.1155/2013/152786 (2013).

3 Chistiakov, D. A., Melnichenko, A. A., Myasoedova, V. A., Grechko, A. V. & Orekhov, A. N. Mechanisms of foam cell formation in atherosclerosis. J Mol Med (Berl) 95, 1153-1165, doi:10.1007/s00109-017-1575-8 (2017).

4 Tabas, I. Macrophage death and defective inflammation resolution in atherosclerosis. Nat Rev Immunol 10, 36-46, doi:10.1038/nri2675 (2010).

5 Luo, Y. et al. Macrophagic CD146 promotes foam cell formation and retention during atherosclerosis. Cell Research 27, 352-372, doi:10.1038/cr.2017.8 (2017).

6 Tall, A. R. Cholesterol efflux pathways and other potential mechanisms involved in the athero-protective effect of high density lipoproteins. Journal of Internal Medicine 263, 256-273, doi:10.1111/j.1365-2796.2007.01898.x (2008).

7 Venkateswaran, A. et al. Control of cellular cholesterol efflux by the nuclear oxysterol receptor LXR alpha. Proc Natl Acad Sci U S A 97, 12097-12102, doi:10.1073/pnas.200367697 (2000).

8 Bischoff, E. D. et al. Non-redundant roles for LXRα and LXRβ in atherosclerosis susceptibility in low density lipoprotein receptor knockout mice. Journal of Lipid Research 51, 900-906, doi:10.1194/jlr.M900096-JLR200 (2010).

9 Collins, J. L. et al. Identification of a Nonsteroidal Liver X Receptor Agonist through Parallel Array Synthesis of Tertiary Amines. Journal of Medicinal Chemistry 45, 1963-1966, doi:10.1021/jm0255116 (2002).

10 Kirchgessner, T. G. et al. Beneficial and Adverse Effects of an LXR Agonist on Human Lipid and Lipoprotein Metabolism and Circulating Neutrophils. Cell Metab 24, 223-233, doi:10.1016/j.cmet.2016.07.016 (2016).

11 Levin, N. et al. Macrophage liver X receptor is required for antiatherogenic activity of LXR agonists. Arteriosclerosis, thrombosis, and vascular biology 25, 135-142, doi:10.1161/01.Atv.0000150044.84012.68

(2005).

12 Wojcicka, G., Jamroz-Wisniewska, A., Horoszewicz, K. & Beltowski, J. Liver X receptors (LXRs). Part I: structure, function, regulation of activity, and role in lipid metabolism. Postepy higieny i medycyny doswiadczalnej (Online) 61, 736-759 (2007).

13. Joseph, S. B. et al. Direct and indirect mechanisms for regulation of fatty acid synthase gene expression by liver X receptors. The Journal of biological chemistry 277, 11019-11025, doi:10.1074/jbc.M111041200 (2002).

14 Joseph, S. B. et al. Synthetic LXR ligand inhibits the development of atherosclerosis in mice. Proc Natl Acad Sci U S A 99, 7604-7609, doi:10.1073/pnas.112059299 (2002).

15 Schultz, J. R. et al. Role of LXRs in control of lipogenesis. Genes & Development 14, 2831-2838, doi:10.1101/gad.850400 (2000).

16 Tibbitt, M. W., Dahlman, J. E. & Langer, R. Emerging Frontiers in Drug Delivery. J Am Chem Soc 138, 704-717, doi:10.1021/jacs.5b09974 (2016).

17 Accardo, A. & Morelli, G. Review peptide-targeted liposomes for selective drug delivery: Advantages and problematic issues. Biopolymers 104, 462-479, doi:10.1002/bip.22678 (2015).

18 Yu, M. et al. Targeted Nanotherapeutics Encapsulating Liver X Receptor Agonist GW3965 Enhance Antiatherogenic Effects without Adverse Effects on Hepatic Lipid Metabolism in Ldlr-/- Mice. Adv Healthc Mater, doi:10.1002/adhm.201700313 (2017).

19 Kelly, K. A., Nahrendorf, M., Yu, A. M., Reynolds, F. & Weissleder, R. In Vivo Phage Display Selection Yields Atherosclerotic Plaque Targeted Peptides for Imaging. Molecular Imaging and Biology 8, 201, doi:10.1007/s11307-006-0043-6 (2006).

20 Park, K. et al. A new atherosclerotic lesion probe based on hydrophobically modified chitosan nanoparticles functionalized by the atherosclerotic plaque targeted peptides. Journal of Controlled Release 128, 217-223, doi:https://doi.org/10.1016/j.jconrel.2008.03.019 (2008).

21 Deosarkar, S. P. et al. Polymeric particles conjugated with a ligand to VCAM-1 exhibit selective, avid, and focal adhesion to sites of atherosclerosis. Biotechnol Bioeng 101, 400-407, doi:10.1002/bit.21885 (2008).

22 Namdee, K. et al. In vivo evaluation of vascular-targeted spheroidal microparticles for imaging and drug delivery application in atherosclerosis. Atherosclerosis 237, 279-286, doi:10.1016/j.atherosclerosis.2014.09.025 (2014).

23 Peters, D. et al. Targeting atherosclerosis by using modular, multifunctional micelles. Proc Natl Acad Sci U S A 106, 9815-9819, doi:10.1073/pnas.0903369106 (2009).

24 Cormode, D. P. et al. Nanocrystal Core High-Density Lipoproteins: A Multimodality Contrast Agent Platform. Nano Letters 8, 3715-3723, doi:10.1021/nl801958b (2008).

25 Zhang, X. Q. et al. Nanoparticles containing a liver X receptor agonist inhibit inflammation and atherosclerosis. Adv Healthc Mater 4, 228-236, doi:10.1002/adhm.201400337 (2015).

26 Zhaorigetu, S., Rodriguez-Aguayo, C., Sood, A. K., Lopez-Berestein, G. & Walton, B. L. Delivery of negatively charged liposomes into the atherosclerotic plaque of apolipoprotein E-deficient mouse aortic tissue. J Liposome Res 24, 182-190, doi:10.3109/08982104.2013.863208 (2014).

27 Binderup, T. et al. Imaging-assisted nanoimmunotherapy for atherosclerosis in multiple species. Science Translational Medicine 11, eaaw7736, doi:10.1126/scitranslmed.aaw7736 (2019).

28 Alaarg, A. et al. A systematic comparison of clinically viable nanomedicines targeting HMG-CoA reductase in inflammatory atherosclerosis. Journal of Controlled Release 262, 47-57, doi:https://doi.org/10.1016/j.jconrel.2017.07.013 (2017).

29 Lobatto, M. E. et al. Atherosclerotic plaque targeting mechanism of long-circulating nanoparticles established by multimodal imaging. ACS Nano 9, 1837-1847, doi:10.1021/nn506750r (2015).

30 Hamzah, J. et al. Specific penetration and accumulation of a homing peptide within atherosclerotic plaques of apolipoprotein E-deficient mice. Proc Natl Acad Sci U S A 108, 7154-7159, doi:10.1073/pnas.1104540108 (2011).

31 Laakkonen, P., Porkka, K., Hoffman, J. A. & Ruoslahti, E. A tumor-homing peptide with a targeting specificity related to lymphatic vessels. Nat Med 8, 751-755, doi:10.1038/nm720 (2002).

32 Peerschke, E. I. et al. Expression of gC1q-R/p33 and its major ligands in human atherosclerotic lesions. Mol Immunol 41, 759-766, doi:10.1016/j.molimm.2004.04.020 (2004).

33 Uchida, M. et al. Protein cage nanoparticles bearing the LyP-1 peptide for enhanced imaging of macrophage-rich vascular lesions. ACS Nano 5, 2493-2502, doi:10.1021/nn102863y (2011).

34 Seo, J. W. et al. (64)Cu-labeled LyP-1-dendrimer for PET-CT imaging of atherosclerotic plaque. Bioconjug Chem 25, 231-239, doi:10.1021/bc400347s (2014).

35 Song, N., Zhao, L., Zhu, M. & Zhao, J. Recent progress in LyP-1-based strategies for targeted imaging and therapy. Drug Deliv 26, 363-375, doi:10.1080/10717544.2019.1587047 (2019).

36 Benne, N. et al. Atomic force microscopy measurements of anionic liposomes reveal the effect of liposomal rigidity on antigen-specific regulatory T cell responses. J Control Release 318, 246-255, doi:10.1016/j.jconrel.2019.12.003 (2020).

37 Marim, F. M., Silveira, T. N., Lima, D. S., Jr. & Zamboni, D. S. A Method for Generation of Bone Marrow-Derived Macrophages from Cryopreserved Mouse Bone Marrow Cells. PLOS ONE 5, e15263, doi:10.1371/journal.pone.0015263 (2010).

38 van Duijn, J. et al. CD8+ T-cells contribute to lesion stabilization in advanced atherosclerosis by limiting macrophage content and CD4+ T-cell responses. Cardiovascular Research 115, 729-738, doi:10.1093/cvr/cvy261 (2018).

39 Mehlem, A., Hagberg, C. E., Muhl, L., Eriksson, U. & Falkevall, A. Imaging of neutral lipids by oil red O for analyzing the metabolic status in health and disease. Nat Protoc 8, 1149-1154, doi:10.1038/nprot.2013.055 (2013).

40 Kritikou, E. et al. Inhibition of lysophosphatidic acid receptors 1 and 3 attenuates atherosclerosis development in LDL-receptor deficient mice. Sci Rep 6, 37585, doi:10.1038/srep37585 (2016).

41 Wezel, A. et al. Complement factor C5a induces atherosclerotic plaque disruptions. J Cell Mol Med 18, 2020-2030, doi:10.1111/jcmm.12357 (2014).

42 Nadkarni, S. K. et al. Measurement of collagen and smooth muscle cell content in atherosclerotic plaques using polarization-sensitive optical coherence tomography. J Am Coll Cardiol 49, 1474-1481, doi:10.1016/j.jacc.2006.11.040 (2007).

43 Out, R. et al. Macrophage ABCG1 Deletion Disrupts Lipid Homeostasis in Alveolar Macrophages and Moderately Influences Atherosclerotic Lesion Development in LDL Receptor-Deficient Mice. Arteriosclerosis, thrombosis, and vascular biology 26, 2295-2300, doi:10.1161/01.ATV.0000237629.29842.4c (2006).

44 Folch, J., Lees, M. & Sloane Stanley, G. H. A simple method for the isolation and purification of total lipides from animal tissues. The Journal of biological chemistry 226, 497-509 (1957).

45 Dickhout, J. G., Basseri, S. & Austin, R. C. Macrophage Function and Its Impact on Atherosclerotic Lesion Composition, Progression, and Stability. Arteriosclerosis, thrombosis, and vascular biology 28, 1413-1415, doi:doi:10.1161/ATVBAHA.108.169144 (2008).

46 Rodriguez-Fernandez, S. et al. Phosphatidylserine-Liposomes Promote Tolerogenic Features on Dendritic Cells in Human Type 1 Diabetes by Apoptotic Mimicry. Front Immunol 9, 253, doi:10.3389/fimmu.2018.00253 (2018).

47 Krishna, S. M. et al. Anionic nanoliposomes reduced atherosclerosis progression in Low Density Lipoprotein Receptor (LDLR) deficient mice fed a high fat diet. J Cell Physiol, doi:10.1002/jcp.26610 (2018).

48 Hosseini, H. et al. Phosphatidylserine liposomes mimic apoptotic cells to attenuate atherosclerosis by expanding polyreactive IgM producing B1a lymphocytes. Cardiovasc Res 106, 443-452, doi:10.1093/cvr/cvv037 (2015).

49 Benne, N. et al. Anionic 1,2-distearoyl-sn-glycero-3-phosphoglycerol (DSPG) liposomes induce antigen-specific regulatory T cells and prevent atherosclerosis in mice. J Control Release 291, 135-146, doi:10.1016/j.jconrel.2018.10.028 (2018).

50 Pujol-Autonell, I. et al. Use of autoantigen-loaded phosphatidylserine-liposomes to arrest autoimmunity in type 1 diabetes. PLoS One 10, e0127057, doi:10.1371/journal.pone.0127057 (2015).

51 Abuchowski, A., McCoy, J. R., Palczuk, N. C., van Es, T. & Davis, F. F. Effect of covalent attachment of polyethylene glycol on immunogenicity and circulating life of bovine liver catalase. The Journal of biological chemistry 252, 3582-3586 (1977).

52 Fernandez, D. M. et al. Single-cell immune landscape of human atherosclerotic plaques. Nature Medicine 25, 1576-1588, doi:10.1038/s41591-019-0590-4 (2019).

53 Wang, Y. et al. Smooth Muscle Cells Contribute the Majority of Foam Cells in ApoE (Apolipoprotein E)-Deficient Mouse Atherosclerosis. Arteriosclerosis, thrombosis, and vascular biology 39, 876-887, doi:10.1161/atvbaha.119.312434 (2019).

54 Bieghs, V. et al. Internalization of modified lipids by CD36 and SR-A leads to hepatic inflammation and lysosomal cholesterol storage in Kupffer cells. PLoS One 7, e34378, doi:10.1371/journal.pone.0034378 (2012)

SUPPLEMENTARY INFORMATION

1. RESULTS

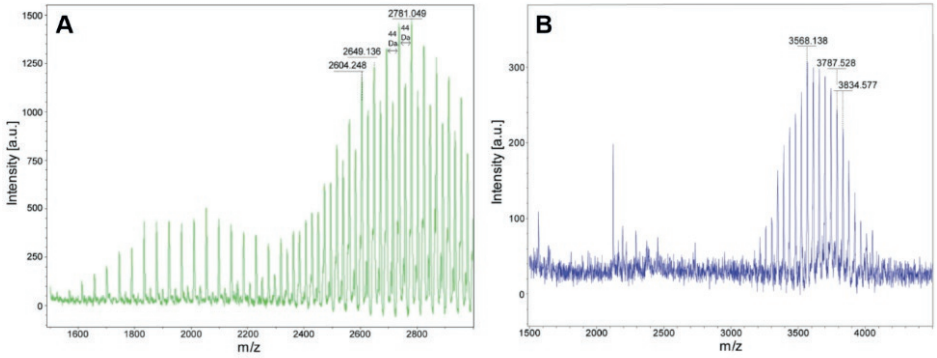

Figure S1. MALDI-MS spectra showing the coupling of DSPE-PEG2000-COOH to cyclic peptide Lyp-1. DSPE-PEG2000-COOH (A) was coupled to cyclic peptide Lyp-1 to produce DSPE-PEG2000-Lyp-1 (B). The mass change between the two spectra corresponds to the successful coupling of the peptide to the lipid.

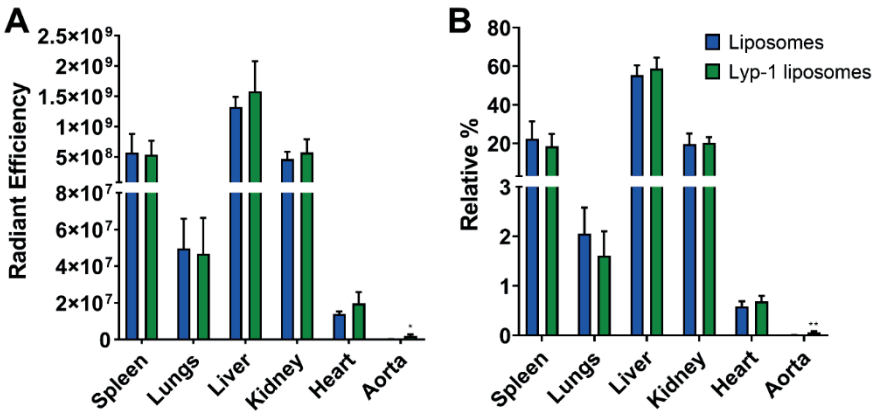

Figure S2. Absolute and relative radiant efficiency of liposomal signal in selected organs in LDLr$^{-/-}$ mice on WTD for 13 weeks, 3 hours after iv injection of non-targeted or Lyp-1 targeted liposomes. Radiant efficiency was measured in spleens, lungs, liver, kidneys, heart, and aorta. (A) Absolute radiant efficient values per organ. (B) The total sum of signals in organs was set to 100%, and the relative radiant efficiency was calculated from this value, n = 5. Graph shows mean + SD, *$p < 0.05$, ***$p < 0.001$ comparing Lyp-1 liposomes to non-targeted liposomes, determined by unpaired t-test.